We are IntechOpen, the world's leading publisher of Open Access books Built by scientists, for scientists

4,800
Open access books available

122,000
International authors and editors

135M
Downloads

Our authors are among the

154
Countries delivered to

TOP 1%
most cited scientists

12.2%
Contributors from top 500 universities

CLARIVATE ANALYTICS BOOK CITATION INDEX INDEXED

WEB OF SCIENCE™

Selection of our books indexed in the Book Citation Index in Web of Science™ Core Collection (BKCI)

Interested in publishing with us?
Contact book.department@intechopen.com

Numbers displayed above are based on latest data collected.
For more information visit www.intechopen.com

On Designing Compliant Actuators Based On Dielectric Elastomers for Robotic Applications

Giovanni Berselli, Gabriele Vassura and Vincenzo Parenti Castelli
University of Bologna
Italy

Rocco Vertechy
PERCRO Laboratory, Scuola Superiore Sant'Anna
Italy

1. Introduction

This chapter reports on advances done in the design of compliant, Dielectric Elastomer based Linear Actuators (DELA).
Dielectric Elastomers (DE) are incompressible deformable dielectrics which can experience deviatoric (isochoric) finite deformations in response to applied large electric fields while, at the same time, alter the applied electric fields in response to the deformations undergone (Kofod et al., 2003; Pelrine et al., 1998; 2000; Toupin, 1956). Thanks to the strong electro-mechanical coupling, DE intrinsically offer great potentialities for conceiving novel solid-state mechatronic devices and in particular actuators. These devices can be profitably used for robotic applications (Bar-Cohen, 2004; Biddiss & Chaua, 2008; Kim & Tadokoro, 2007; Plante & Dubowsky, 2008). In fact, concerning conventional actuation technologies (such as electric motors), some basic problems remain unaddressed or, at least, improvable, such as:

- The need to increase flexibility and simplify design solutions. For an important number of applications, conventional systems are too heavy, inefficient (in terms of high power consumptions), too expensive and still relatively complex.
- The need to design human-friendly machines (Bicchi & Tonietti, 2004). In order to achieve highly precise position control, many industrial mechatronic systems (especially industrial robots) are designed to be very fast and stiff and thus potentially dangerous to humans. A possible way to greatly increase safety, is the design of robotic structures which are less precise but more compliant when compared to the traditional ones. To this respect, it is possible to concentrate the compliance in the actuated joints by using compliant (soft) actuators.
- The need for modern robots to interact with unstructured environments and to actively control force and stiffness at the contact interface. A promising approach is to rely on a mechanical system that is inherently compliant and to use active control strategies to vary this compliance (Biagiotti et al., 2004). The main advantages are a lower request both on actuator and controller bandwidth and improved stability (Paul & Shimano, 1976; Williamson, 1993).

- The need to develop alternative actuators to overcome design limitations which are imposed in few but very important specific applications. For instance, electromagnetic actuators cannot be used in the presence of the high magnetic fields generated by Magnetic Resonance Imaging (MRI) devices. Nevertheless, the possibility to accomplish manipulation tasks within an MRI environment would highly improve the diagnostic capabilities of this technology (Koseki et al., 2007).

Thanks to their intrinsic compliance, lightness, pliability, and low cost, actuators based on DE can be an explorable solution when trying to assess or improve the aforementioned issues.
DELA are usually composed of one or more DE shaped as a thin membrane (film) and a flexible supporting frame.
This chapter proposes a methodology that allows the modification of the available thrust as a function of the actuator length at will of the designer and, in particular, to obtain constant force actuators. The design procedure is divided in two steps: 1) optimization of the DE electromechanical parameters 2) design of the flexible frame. The supporting frame is conceived as a compliant mechanism (Howell, 2001) and it makes use of the stiffness characteristics of slider-crank mechanisms with elastic revolute pairs to be coupled (in symmetric or axis-symmetric configurations) with films of different geometries. Three actuator concepts are proposed which highlight the efficacy of the proposed method, in particular Rectangular DELA (1(a), 1(d)), Diamond DELA (1(b), 1(e)) and Conical DELA (1(c), 1(f)).

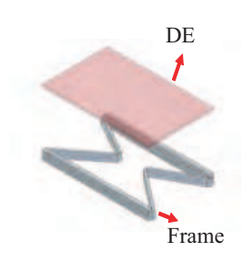

(a) Rectangular DELA.

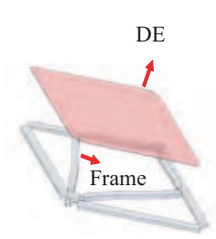

(b) Diamond DELA.

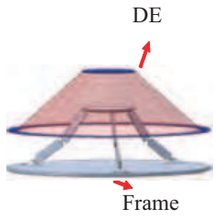

(c) Conical DELA.

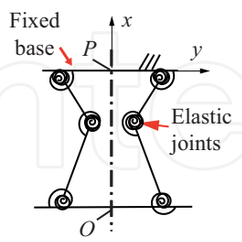

(d) Rectangular DELA frame schematic.

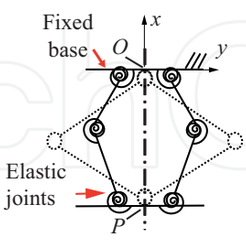

(e) Diamond DELA frame schematic.

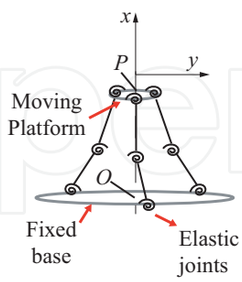

(f) Conical DELA frame schematic.

Fig. 1. DELA concepts.

2. Background on Dielectric Elastomer Actuators

For actuation usage, DE can be shaped in thin films which are firstly prestretched then coated with compliant electrodes on both sides and piled one on the other to form an Electrically Deformable Film (EDF). An EDF can be mono or multi layered (Fig. 2). Activation of the EDF via the placement of an electric field, E_z, acting in the film thickness direction (z direction, Fig. 2) or, equivalently, of differential electric potentials (hereafter also called voltages, V) between the electrodes can induce a film area expansion and, thus, point displacements which can be used to produce useful mechanical work (whenever forces are applied to such points). The term EDF simply identifies a dielectric, hyperelastic, and incompressible isotropic membrane (the DE) placed between two compliant electrodes.

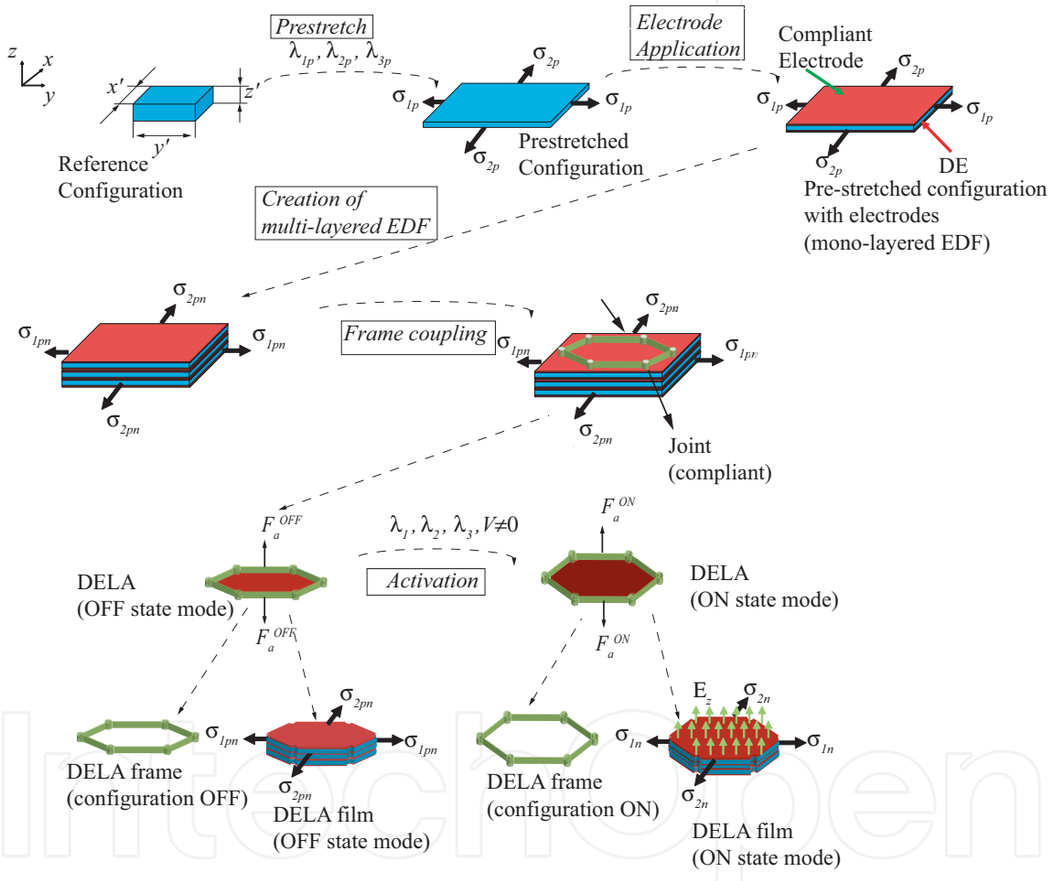

Fig. 2. DELA production steps.

Usually, DE-based actuators are obtained by first *uniformly* prestretching the DE (which is necessary since the film has negligible flexural rigidity) and then by coupling some segment of its boundary to some portion of a flexible supporting frame, either an elastic structural element (Kofod et al., 2006; Pei et al., 2003), for instance a helical spring, or a compliant mechanism (Berselli et al., 2008; 2009a; Plante, 2006; Vogan, 2004; Wingert et al., 2006), for instance a four-bar mechanism with elastic revolute joints. Figure 2 summerizes the conceptual steps carried

out for the production of DELA with generic geometry, that is DE prestretch, compliant electrode application (of single EDF layers), assembly of a multi-layered EDF and coupling with a frame of given geometry. In the following, the term *OFF state mode* and *ON state mode* will identify every actuator working condition where $V = 0$ and $V \neq 0$ respectively.
The major roles of the flexible polymeric frame are:

- to prevent the development of current arcs around the EDF border;
- to protect the EDF edges;
- to provide a firm support for the application of external forces;
- to coerce the EDF expansion in preferred directions;
- to maintain the EDF in a tensioned state so as to prevent wrinkling effects;
- to modify the overall actuator stiffness (EDF + frame) by using the frame own stiffness.

The actuator stiffness identifies the ratio among the variation of the actuator available thrust with respect to the variation of its length. In particular, specific compliant frames (Fig. 1) can be designed in order to achieve a constant force for a given range of actuator stroke and therefore a nearly naught stiffness. Constant force actuators can be beneficially employed in those applications that require constant but controllable output force over a given range of motion. For example, in grasping and manipulation applications, the desired grasp force might change with respect to the weight of the object to be manipulated. An actuator that provides a constant force would be capable of applying that given force even in presence of small deflections or positioning errors thus minimizing the control effort.
Different solutions for possible frame geometries have been proposed in the literature (Bolzmacher et al., 2004; Kofod & Sommer-Larsen, 2005; Lochmatter, 2007; Plante, 2006; Vogan, 2004) which make use of EDF in planar or spatial shapes (Fig. 3). Some of these shapes can be analytically solved in terms of EDF force vs EDF displacement (Plante (2006)) whereas most of them have to be studied through either Finite Element (FEM) analysis or experiments.

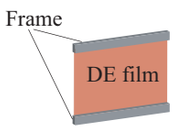

(a) Rectangular DELA (planar).

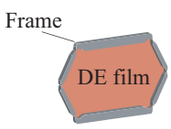

(b) Hexagonal shaped DELA (planar).

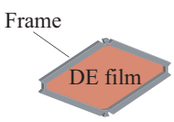

(c) Diamond DELA (planar).

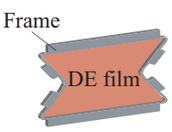

(d) Bow-tie DELA (planar).

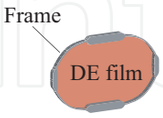

(e) Elliptical DELA (planar).

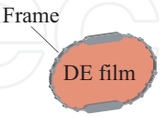

(f) Leaf spring DELA (planar).

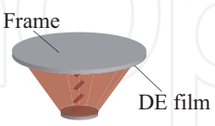

(g) Conical DELA (spatial).

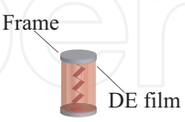

(h) Cylindrical DELA (spatial).

Fig. 3. DELA prototype for possible frame geometries.

3. General aspects of frame design

3.1 Compliant frame effect on the actuator performance

According to a simplified one-dimensional model, also adopted by Plante (2006), a DELA actuator can be considered as a set of two interacting springs: one, the EDF, operating under tension, the other, the frame, operating under compression. In general, the film deformation produces a variation of the actuator length $x = |(P - O)|$, where P and O are two points of the actuator (Figs. 1, 4(a), 4(b)), and a force having the same direction as that of the motion can be supplied to an external user.

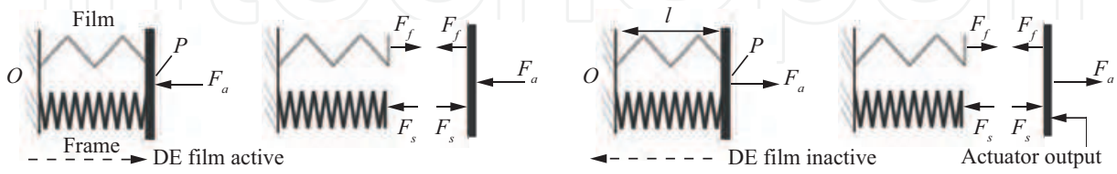

(a) Negative thrust: $|F_f| < |F_s|$ (b) Positive thrust: $|F_f| > |F_s|$

Fig. 4. Forces acting in the system in the ON state mode (a) and in the OFF state mode (b).

This force, called the actuator available thrust, F_a, can be represented as in Fig. 4 and is the resultant of two internal forces:

- The frame reaction force F_s due to the frame own stiffness, that is a function of the actual frame configuration. The compliant frame behaves, in general, like a non-linear compression spring coupled in parallel with the EDF.
- The EDF force F_f which represents the resultant force in the direction of the actuator motion due to the stress field arising in the EDF. This field depends on the amount of given prestretch, on the applied electric potential (voltage), and on the actuator configuration. In a one-dimensional model, where material viscoelasticity, creep and hysteresis are ignored, the film behaves, in general, as a non-linear tension spring. Under a step voltage variation the film force F_f undergoes a finite decrease, dependent on the magnitude of the applied voltage (see Fig. 5).

The available thrust F_a is therefore given by the difference between the film and the frame forces:

$$F_a(x, V) = F_f(x, V) - F_s(x) \tag{1}$$

Conventionally, F_a is the force that an external user supplies to the actuator.

Figure 5 shows qualitative diagrams of Force vs actuator Length (FL) curves concerning internal forces F_f and F_s, adopting a representation methodology widely used in the study of interacting elastic structures where the moduli of the forces are shown.

The *continuous* curve F_f^{off} represents the film force F_f in the inactive state whereas the *dotted* curve s represents the frame reaction force F_s.

In the OFF state mode (curve F_f^{off}), after the coupling of the prestretched film and the precompressed frame, the achieved equilibrium position is represented by point A. In this condition (no applied load and no applied voltage), the actuator initial length is x_0. The displacements imposed on the one-dimensional springs representing the film and the frame are given respectively by $|x_0 - x_{0f}|$ and $|x_{0s} - x_0|$, where x_{0f} is the free length of the EDF and x_{0s} is free length of the frame. Point A is taken as the reference point for the measurement of the

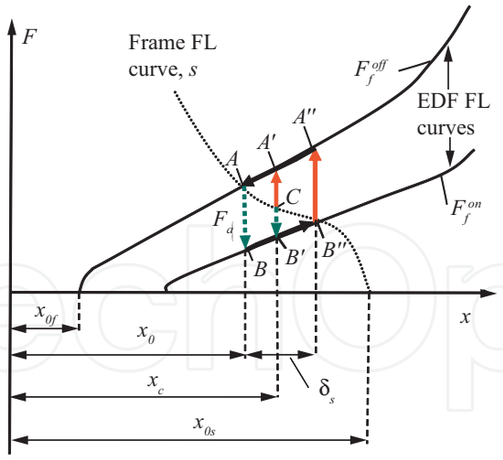

Fig. 5. FL relationship showing the effect of the film/frame coupling.

actuator stroke δ.
On the other hand, the *continuous* curve F_f^{on} represents the relationship between F_f and the actuator length, in the case of film activation under constant voltage. Point B represents the new value of F_f upon a step voltage rise, starting from point A. The distance between points A and B symbolizes the available thrust F_a. In this condition $|F_f| < |F_s|$ and the actuator output can move outward (Fig.4(a)). If the actuator output is free to move (no external load), the actuator can now reach a new equilibrium position represented by point B'' and δ_s represents the maximum stroke obtainable with a frame characterized by a FL profile like curve s.
In any intermediate position defined by x, points C and B' represent respectively forces F_s and F_f^{on}; in this condition, the available thrust is equal to the distance $\overline{B'C}$. If, at any point along the stroke, the excitation voltage is suddenly removed, the force acting on the film abruptly passes from point B' to point A', thus obtaining $|F_f| > |F_s|$ (Fig. 4(b)) and an available thrust acting in the opposite direction with absolute value equal to the distance $\overline{A'C}$. According to the adopted convention on the force sign, the available thrust can be plotted as in Fig. 6(a)

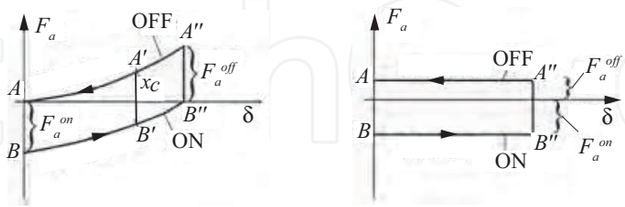

Fig. 6. Actuator force vs stroke relationship; real behavior (a) and ideal behavior (b).

The force profiles of F_a in the active and inactive states (F_a^{on} and $F_a{}^{off}$ respectively) can be modified by working on the frame design depending on the application requirements.
It can be seen from Fig. 6(a) that in general F_a is changing along the stroke δ, either when the actuator state is ON or OFF. However, it has been noticed (Pedersen et al., 2006) that a general purpose actuator should rather provide a constant thrust along its stroke (as in Fig. 6(b)).

3.2 Achievement of constant force actuators

Assuming the film electromechanical characteristics as given, the compliant frame stiffness can be designed in order to modify the curve s (Fig. 5) and obtain an actuator capable of providing a constant force over a given range of motion.

Let us suppose the EDF is coupled with a compliant mechanism whose elastic reaction force decreases as the actuator length x increases. In a one-dimensional model, such a frame can be conceived as a negative stiffness spring acting in parallel with the EDF. If this negative stiffness perfectly matches the EDF stiffness, a constant output force can be obtained.

The operating principle is illustrated in Fig. 7 where three different curves for F_s are represented assuming that the initial length of the actuator x_0 and the maximum obtainable stroke δ_s are invariant.

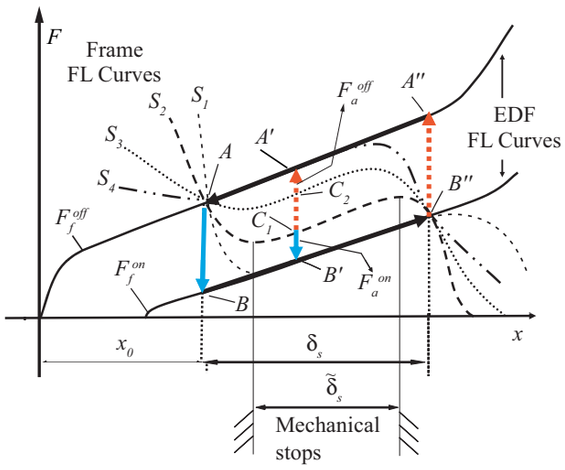

Fig. 7. FL relationship showing the "negative stiffness" effect.

Let us consider first, a frame FL curve depicted by the curve S_2, where the frame configuration is defined as the length $x = |P - O|$ (as previously defined). It can be seen that, for a large part of the stroke, the actuator available thrust, F_a, maintains a constant value, ${F_a}^{off}$, equal to the distance $\overline{A'C_1}$ if the EDF is deactivated.

In Fig. 7, ${F_f}^{off}$ and ${F_f}^{on}$ are approximated as parallel (as it happens for some actuator geometries (Berselli et al., 2008; 2009a; Wingert et al., 2006)). In such a case the same frame can be used also to obtain a constant available thrust ${F_a}^{on}$, equal to the distance $\overline{B'C_1}$ when the EDF is activated. If the actuator is required to supply a larger thrust when the EDF is active (actuator ON-state mode), a frame FL profile alike curve S_3 can be chosen, so as to increase ${F_a}^{on}$ from $\overline{B'C_1}$ to $\overline{B'C_2}$ (and consequently to decrease ${F_a}^{off}$). The OFF-state mode actuator thrust ${F_a}^{off}$ is maximized by designing a frame that provides a FL profile alike curve S_1 whereas the ON-state mode actuator thrust ${F_a}^{on}$ is maximized by designing a frame that provides a FL profile alike curve S_4. In this situation, however, no restoring force can pull back the actuator to its initial position when the voltage is switched off (actuator on OFF-state mode) and a returning device has to be provided. In practice, for applications requiring control via bidirectional forces, two identical actuators can be employed in an agonistic-antagonistic configuration.

Note that the actuator stroke can be limited to $\widetilde{\delta_s}$ by purposely designed mechanical stops in order to prevent motion in undesired regions (e.g. regions where the thrust is not constant).

4. Possible frame designs

In order to achieve a constant force, provided that F_f monotonically increases as the actuator length increases, the frame should provide a negative force F_s whose value decreases along the same range (i.e the frame stiffness, $K_s = dF_s/dx$ should be negative). In general, this behavior is exhibited by mechanisms characterized by unstable equilibrium positions along their motion. For example, a bi-stable element presents an unstable equilibrium position (UEP) between two stable equilibrium positions (SEP) and can act as a negative stiffness spring over a given range of motion. Considering the FL profile of a bi-stable mechanism, the equilibrium positions occur at location where $F_s = 0$. In general, an equilibrium position is stable if the input force/moment increases as the generalized coordinate, x, increases (i.e. $K_s = dF_s/dx > 0$). On the other hand, the equilibrium position is unstable if the input force/moment decreases as the generalized coordinate increases (i.e. $K_s = dF_s/dx < 0$). Therefore a bi-stable element can act as a negative stiffness spring over a given range of motion and specifically around the UEP. Previously published solutions employed compound structure frames (i.e. additional mechanisms were employed in order to modify the FL profile of a given actuator). In particular, Plante (2006) and Vogan (2004) proposed the use of a bi-stable "snap through buckled beam" element or the use of an "over the center" device to be coupled with a "diamond" shaped supporting compliant mechanism with negligible joint stiffness. The critical aspects of such designs are related most of all to the use of non linear tension springs (Plante, 2006) or lateral instability due to beam buckling (Vogan, 2004).

(a) (b) (c)

Fig. 8. Slider-Crank Compliant Mechanism (SCCM). Undeflected (a) and deflected (b) configuration. PRBM (c)

As an alternative design, here it is proposed to make use of the stiffness characteristic achievable with the Slider-Crank Compliant Mechanism (SCCM). A schematic of an SCCM in undeflected and deflected configuration is shown in Fig. 8(a) and Fig. 8(b). The Pseudo Rigid Body Model (PRBM) (Howell, 2001) of the same compliant mechanism is depicted in Fig. 8(c) where r_1 and r_2 are the crank and the connecting-rod lengths respectively, e is the slider-crank mechanism eccentricity, x is the mechanism length (i.e. the distance between the points O and P), K_1, K_2, K_3 are the spring constants of the compliant joints (Howell, 2001), ϑ_1 and ϑ_3 are the crank angle and connecting rod angular positions measured with respect to the actuator direction of motion ($\vartheta_2 = \vartheta_1 - \vartheta_3$), and ϑ_{10} ,ϑ_{20} ,ϑ_{30} are the undeflected angular positions of the flexural pivots ($\vartheta_{20} = \vartheta_{10} + \vartheta_{30}$).

Let us define the force F_s as the SCCM reaction force due to its own stiffness, that is a function of the actual mechanism configuration. Invoking the principle of the superimposition of the effects, the force F_s is given by:

$$F_s = F_1 + F_2 + F_3 \tag{2}$$

where the forces F_1, F_2 and F_3 are due to the deflection of the torsional springs with stiffness K_1, K_2 and K_3 respectively. Let us consider separately the contribution of each stiffness K_1, K_2 and K_3. At first, neglect the contribution of torsional springs with stiffnesses K_1 and K_2, such that $F_s = F_3$.

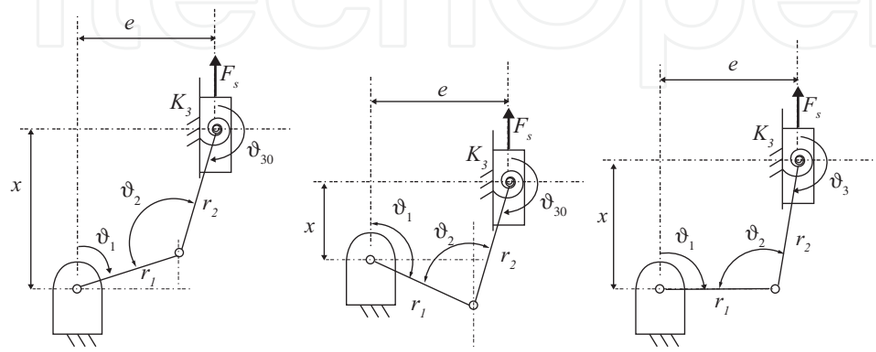

Fig. 9. SCCM. First stable position (a), second stable position (b), unstable position (c).

In such a situation, the resulting mechanism is depicted in Fig. 9(a) where the torsional spring with stiffness K_3 is represented in its undeflected position. Such mechanism is bi-stable. In fact two SEP are reached when the torsional spring is undeflected. If Figure 9(a) represents the first SEP, another SEP is reached when the connecting rod reaches a configuration parallel to its configuration at the first SEP. Therefore, Figure 9(b) represents the second SEP. An UEP is reached when the rocker arm is perpendicular to the slider direction of motion as depicted in Fig. 9(c).

Let us now neglect the contribution of the torsional spring with stiffness K_3 and, therefore, consider the contribution of the forces F_1 and F_2 only. Define $F_{12} = F_1 + F_2$. The resulting mechanism is a possible topology of a compliant mechanism that can supply a nearly constant-force if suitably dimensioned. The dimensions of the PRBM (i.e. the values of K_1, K_2, r_1, r_2, e, and the undeflected angular positions of the joints) resulting in a constant force may be found by minimizing the variation of the output force over the given input displacement as it will be shown in the next paragraph.

It is clear that, if coupled with DELA of different shapes, SCCM can be used to tailor the actuator stiffness to a given application and, in particular, design constant force actuators. Depending on the SCCM design, the actuator can work bidirectionally or monodirectionally (Berselli et al., 2009a) depending on whether or not the frame own stiffness provides a restoring force that brings back the actuator to an initial position when the EDF is deactivated. As a proof of concept, let us consider the mechanisms shown in Fig. 10(a) that will be referred to as Delta Element. Figure 10(b) represents a particular case where $e = 0$.

The Delta Element is in fact a parallel mechanism. However if the loads are directed along the x direction (shown in Fig. 10(a)) half mechanism can be modeled as an SCCM. The Delta Element can be coupled to every DE planar actuator to form a constant force actuator. Fig.

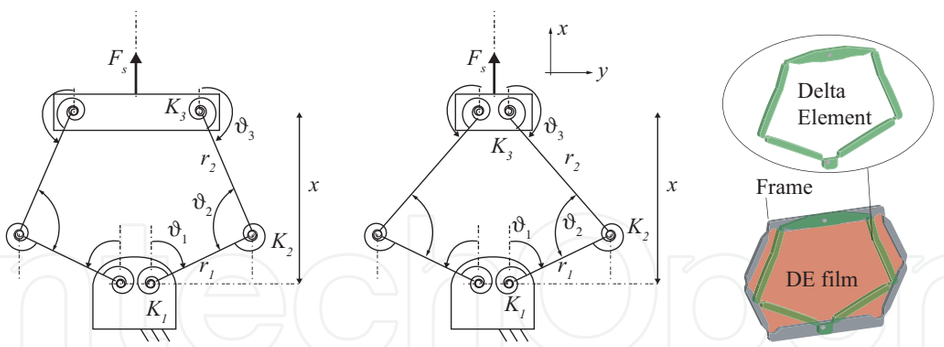

(a) Eccentric Delta Element (b) Delta Element (c) Delta element coupled with an hexagonal DELA

Fig. 10. Different possible configuration of compliant frames

10(c) shows a Delta Element coupled with a hexagonal DELA.
Qualitatively the behavior of the SCCM coupled with the EDF (Delta Element or other possible frame configuration based on the same concept) is shown in Fig. 11 where the contributions of the single forces F_3 and F_{12} are also depicted. The curve S_6 represents the total force $F_s = F_{12} + F_3$. Note that, given the desired stiffness of the actuator as a whole, that is EDF coupled with the SCCM (a null stiffness being represented in Fig. 11), the actuator thrust in the ON and OFF state modes can be adjusted by working on the force F_{12} only. In fact the curve S_6' which maximizes the thrust in the ON state mode has been obtained through an SCCM which provides a reaction force $F_s = F_3 + F_{12}'$.

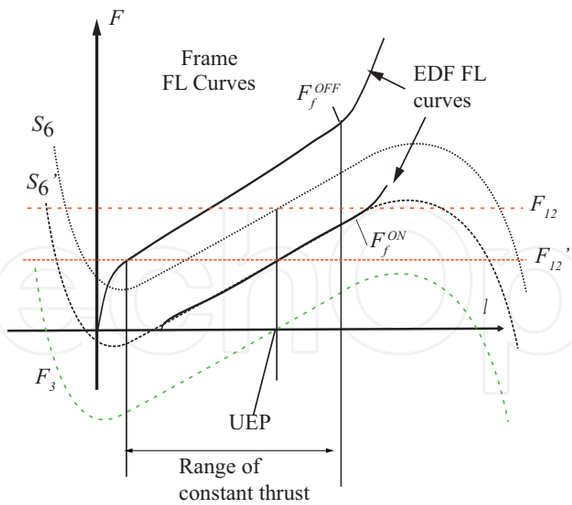

Fig. 11. Effect of the SCCM on the overall actuator stiffness.

5. Mathematical model of the Dielectric Elastomer film force

For design purposes DE can be considered as incompressible, hyper-elastic linear dielectrics whose electric polarization is fairly independent of material deformation (Berselli et al., 2008;

2009a; Kornbluh et al., 1995; Pelrine et al., 1998). For such elastomers, EDF activation generates an electric field, $E = V/z$ (V being the activation voltage applied between the EDF electrodes and z being the actual thickness of the DE film amid the EDF electrodes), and an electrically-induced Cauchy stress, $\sigma_{em} = \epsilon E^2$ (ϵ being the DE electric permittivity), both acting in the DE film thickness direction. As a consequence, the mechanical stress field in a stretched and activated DE, which is free to deform in its thickness direction, is given by the following relationships:

$$\sigma_1 = -p + \lambda_1 \frac{\partial \psi}{\partial \lambda_1}; \qquad \sigma_2 = -p + \lambda_2 \frac{\partial \psi}{\partial \lambda_2}; \qquad \sigma_3 = -p = -\epsilon E^2 = \frac{-\epsilon V^2}{z^2} = \frac{-\epsilon V^2}{{\lambda_3}^2 {z'}^2} \quad (3)$$

where λ_i and σ_i $(i = 1, 2, 3)$ are, respectively, the principal stretches and Cauchy stresses (the 3-rd principal direction coinciding with the film thickness direction), $\psi = \psi(\lambda_1, \lambda_2, \lambda_3)$ defines the DE strain-energy function (Ogden, 1972), and $z' = z/\lambda_3$ is the unstretched DE film thickness (in the reference configuration).
Considering an Ogden model for the constitutive behavior of incompressible rubber-like materials, it is postulated that the strain-energy function ψ has the form:

$$\psi = \psi(\lambda_1, \lambda_2) = \sum_{p=1}^{k} \frac{\mu_p}{\alpha_p} (\lambda_1^{\alpha_p} + \lambda_2^{\alpha_p} + \lambda_1^{-\alpha_p} \lambda_2^{-\alpha_p} - 3) \quad (4)$$

where k is the model order and μ_p, α_p are material parameters to be determined experimentally, that is curve fitted over experimental stress/stretch data. In his work, first order models are used ($k = 1, \alpha_1 = \alpha, \mu_1 = \mu$). Note that ψ is function of λ_1 and λ_2 only because incompressibility is assumed ($\lambda_3 = 1/\lambda_1\lambda_2$).
When $V = 0 \Rightarrow \sigma_3 = 0$, which is, in fact, the applied boundary condition for the EDF in the OFF state mode.

5.1 Rectangular actuators

Rectangular actuators are based on a rectangular mono-axially prestretched DE coupled to two rigid beams (Fig. 3(a)). Let us define (Fig. 12(a)) x' and y' as the EDF planar dimensions in the reference configuration (unstretched EDF) whereas x and y_p are EDF planar dimensions in the actual configuration. Note that y_p remains constant during actuator functioning. It is supposed that the DE deformation can be described by a pure shear deformation [1]. A principal prestretch $\lambda_{2p} = y_p/y'$ is applied in the y direction. The prestretch λ_{2p} is an independent design parameter. The points O and P are two points of the DELA frame placed, for instance, on its axis of symmetry and lying on the two opposite rigid beams.
As depicted in Fig. 12, in such actuators, activation of the EDF makes it possible to control the relative distance x (hereafter also called "DE length" or "actuator length") of the points O and P, which are supposed to be the points of application of the (given) external forces F_f acting on the actuator boundary. The DE deformation state (pure shear), (Ogden, 1972) is characterized by the following principal stretches:

$$\lambda_1 = \frac{x}{x'}; \qquad \lambda_2 = \lambda_{2,p}; \qquad \lambda_3 = \frac{1}{\lambda_1\lambda_2} = \frac{z}{z'} \quad (5)$$

[1] According to the definition given by Ogden (1972), a pure shear deformation is characterized by the constancy of one principal stretch (for instance λ_2). A pure shear deformation can be achieved for infinitely wide EDF (i.e. for $y_p >> x \; \forall \; \Omega(t)$ where $\Omega(t)$ are the possible configurations of the EDF in working condition.

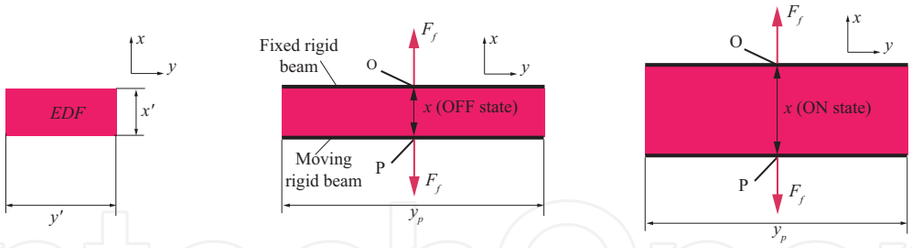

(a) Unstretched EDF.

(b) Rectangular DELA, schematic (OFF-state mode).

(c) Rectangular DELA, schematic (ON-state mode).

Fig. 12. Rectangular DELA.

Considering the xy plane, the principal stretch/stress directions are respectively aligned and orthogonal to the line joining the points O and P. Consequently, the mechanical stress field in a prestretched and activated DE, which is free to deform in its thickness direction, is given by Eq. 3.

Let us derive the expression of the external force $F_f = F_f(x, V)$ that must be supplied at O and P (and directed along the line joining these points) to balance the DE stress field at a given (fixed) generic configuration x of the actuator:

$$F_f(V,x) = z y_p \sigma_1(x,V) = y_p z' \lambda_3 \lambda_1 \frac{\partial \psi}{\partial \lambda_1} - \epsilon V^2 \frac{y_p}{z} = \frac{y_p z'}{\lambda_{2,p}} \frac{\partial \psi}{\partial \lambda_1} - \epsilon V^2 \frac{y_p \lambda_{2,p}}{z' x'} x \tag{6}$$

which, by convention, is positive if directed according to the arrows depicted in Fig. 12. Conventionally, F_f is the force that an external user supplies to the actuator.

It can be noted that $F_f(V,x)$ can be decomposed in two terms:

$$F_f^{off}(x,0) = F_f^{off}(x) = \frac{y_p z'}{\lambda_{2,p}} \frac{\partial \psi}{\partial \lambda_1} \tag{7}$$

and

$$F_f^{em}(x,V) = -\epsilon V^2 \frac{y_p \lambda_{2,p}}{z' x'} x \tag{8}$$

The force F_f^{off} is the force supplied by an external user to the actuator when the voltage $V = 0$ (it has been termed as the DE *film force* in the OFF state mode). The force F_f^{on} is the force supplied by an external user to the actuator when the voltage $V \neq 0$. The DE *film force* in the ON state mode is given by:

$$F_f^{on}(x,V) = F_f^{off}(x) + F_f^{em}(x,V) \tag{9}$$

The "electrically induced" term F_f^{em} has the dimension of a force and is usually referred to as *Maxwell force* (Kofod & Sommer-Larsen, 2005; Plante, 2006) or *actuation force*.

Equation 8 shows that: 1) the "force" F_f^{em} does not depend on the strain energy function which is chosen to describe the material hyperelastic behavior 2) the "force" F_f^{em}, in case of rectangular actuators, is affected by prestretch (for the same undeformed DE geometry). In the following, the electrically induced force F_f^{em} will also be called *force difference* or *actuation force*.

5.2 Diamond actuators

Diamond actuators are based on a bi-axially prestretched lozenge shaped DE coupled to a frame made by a four-bar linkage mechanism having links with equal length, l_d (Fig. 13(c)). The DE is attached all over the frame border. Principal prestretches $\lambda_{1p} = x_p/x'$ and $\lambda_{2p} = y_p/y'$ are applied in the x and y directions and are independent design parameters. Let us define (Fig. 13(a)) x' and y' as the EDF planar dimensions in the reference configuration (unstretched EDF) whereas x_p and y_p are EDF planar dimensions in prestretched configuration. The coupling with the frame is done when the distance OP is equal to x_p (x_p can be chosen as desired) where O and P are the centers of two opposing revolute pairs of the four-bar mechanism (as shown in Fig. 13). In particular, it has been chosen $x = x_p$ for the EDF in the OFF state mode (Fig. 13(b)).

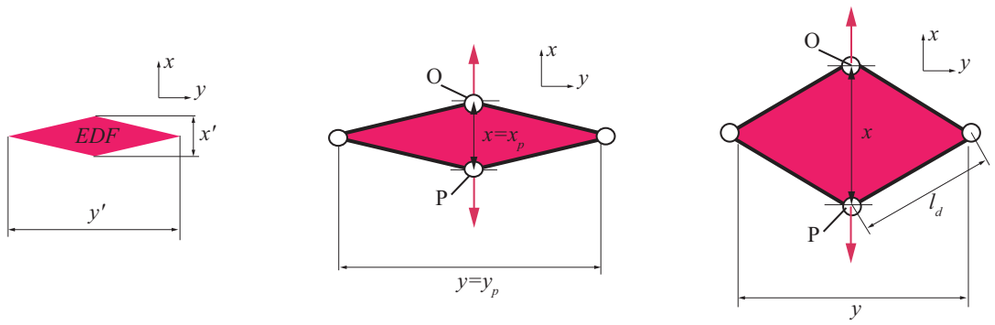

(a) Unstretched EDF. (b) Diamond DELA, schematic (OFF-state mode). (c) Diamond DELA, schematic (ON-state mode).

Fig. 13. Diamond DELA).

In such actuators, activation of the EDF makes it possible to control the relative distance x (hereafter also called "DE length" or "actuator length") of the points O and P, which are supposed to be the points of application of the (given) external forces F_f acting on the actuator boundary.

By construction, when coupled with a four-bar mechanism having links of equal length, lozenge-shaped EDF expand uniformly without changing their edge length l_d and principal stretch/stress directions. Thus, their deformation state is characterized by the following principal stretches:

$$\lambda_1 = \frac{x_p}{x'}\frac{x}{x_p} = \lambda_{1,p}\frac{x}{x_p}; \quad \lambda_2 = \frac{y_p}{y'}\frac{y}{y_p} = \lambda_{2,p}\frac{y}{y_p} = \lambda_{2,p}\sqrt{(4l_d^2 - x^2)/(4l_d^2 - {x_p}^2)}; \quad \lambda_3 = \frac{1}{\lambda_1\lambda_2} = \frac{z}{z'} \tag{10}$$

where the following kinematic relations can be easily found by the position analysis of the four-bar linkage machanism with links of equal length and observing that the displacements of both EDF boundary and frame must be identical, that is:

$$y = \sqrt{(4l_d^2 - x^2)} \qquad y_p = \sqrt{(4l_d^2 - {x_p}^2)} \tag{11}$$

Considering the xy plane, the principal stretch/stress directions are respectively aligned and orthogonal to the line joining the points O and P. Consequently, the mechanical stress field in

a prestretched and activated DE, which is free to deform in its thickness direction, is given by Eq. 3.
Let us now derive the expression of the external force that must be supplied at O and P, and directed along the line joining these points, to balance the DE stress field at a given (fixed) generic configuration x of the actuator. Because of symmetry, a quarter of the actuator can be schematized as in Fig. 14.

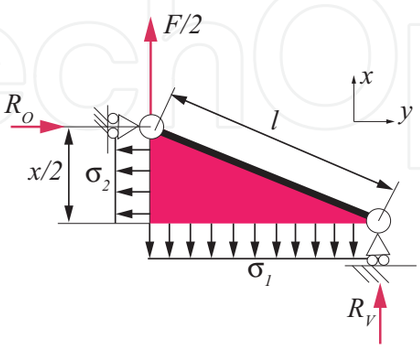

Fig. 14. Diamond DELA, force equilibrium.

The force F_f can be found using the equilibrium equations:

$$\frac{F_f}{2} + R_V = B_1; \qquad R_O = B_2; \qquad \frac{F_f}{2}\frac{y}{2} + R_o\frac{x}{2} = B_2\frac{x}{4} + B_1\frac{y}{4}; \tag{12}$$

where

$$B_1 = z\frac{y}{2}\sigma_1(x,V); \qquad B_2 = z\frac{x}{2}\sigma_2(x,V); \tag{13}$$

therefore

$$F_f = B_1 - B_2\frac{x}{y} = \frac{z'}{\lambda_1\lambda_2}\frac{y}{2}\lambda_1\frac{\partial\psi}{\partial\lambda_1} + \frac{z'}{\lambda_1\lambda_2}\frac{y}{2}\epsilon E^2 - \frac{z'}{\lambda_1\lambda_2}\frac{x}{2}\frac{x}{y}\lambda_2\frac{\partial\psi}{\partial\lambda_2} - \frac{z'}{\lambda_1\lambda_2}\frac{x}{2}\frac{x}{y}\epsilon E^2 \tag{14}$$

which, by convention, is positive if directed according to the arrows depicted in Fig. 13. It can be noted that $F_f(V,x)$ can be decomposed in two terms:

$$\begin{aligned} F_f^{off}(x,0) = F^{off}(x) &= z\lambda_1\frac{\partial\psi}{\partial\lambda_1}\frac{y^2}{4} - z\lambda_2\frac{\partial\psi}{\partial\lambda_2}\frac{x}{2}\frac{x}{y} \\ &= \frac{z'}{2}\left(\frac{\sqrt{(4l_d^2 - {x_p}^2)}}{\lambda_{2,p}}\frac{\partial\psi}{\partial\lambda_1} - \frac{x x_p}{\lambda_{1,p}\sqrt{(4l_d^2 - x^2)}}\frac{\partial\psi}{\partial\lambda_2}\right) \end{aligned} \tag{15}$$

and

$$F_f^{em}(x,V) = z\frac{y}{2}\left(\frac{-\epsilon V^2}{{\lambda_3}^2 {z'}^2}\right) + z\frac{x}{2}\frac{x}{y}\left(\frac{-\epsilon V^2}{{\lambda_3}^2 {z'}^2}\right) = \frac{-\epsilon V^2}{z'}\lambda_{1,p}\lambda_{2,p}\frac{x(2l_d^2 - x^2)}{x_p\sqrt{(4l_d^2 - {x_p}^2)}} \tag{16}$$

The force F_f^{off} is the film force in the OFF state mode whereas the film force in the ON state mode is given by:

$$F_f^{on}(x,V) = F_f^{off}(x) + F_f^{em}(x,V) \tag{17}$$

As stated for the rectangular actuators, the term expressed by F_f^{em} can be interpreted as an "electrically induced force" due to DE activation.

5.3 General remarks on the DE film models

Let us define: 1) the parameter $\zeta = x_b/x_f \leq 1$, where x_b is the initial actuator length and x_f is the final actuator length ($\delta = x_f - x_b = x_b(\zeta^{-1} - 1)$, being the actuator stroke); 2) the actuation force relative error as:[2]

$$e_T = [max(F_f^{em}(x))/min(F_f^{em}(x)) - 1] \quad \text{within } x_b \leq x \leq x_f \tag{18}$$

Different considerations can be drawn for the rectangular and the diamond actuators:

- Rectangular actuator. The actuation force is given by Eq. 8. Considering the DE parameters as fixed and given a maximum actuation voltage V_{max}:

$$e_T^{rectangular} = F_f^{em}(x_f)/F_f^{em}(x_b) - 1 = \frac{1}{\zeta} - 1 \tag{19}$$

  where it can be seen that the actuation force relative error depends on ζ and increases as ζ decreases being null for actuators presenting a null stroke. A possible way to keep $e_T = 0$ is by setting $V^2 = \frac{\Delta F_d}{C_{ps} x}$ where ΔF_d is the desired force difference, $C_{ps} = \frac{y_p \lambda_{2p} \epsilon}{z' x'}$. The information about the actual DE position x must be obtained with appropriate sensory systems or using the methods described in Jung et al. (2008) and fed back to a voltage controller. Obviously the actuation source should be capable of actively controlling the voltage.
- Diamond actuators. The actuation force is given by Eq. 16.
  Let us consider the adimensional parameter $\chi = x/l_d$ which uniquely identifies the lozenge configuration ($\chi_b = x_b/l_d, \chi_f = x_f/l_d, \zeta = \chi_b/\chi_f, \chi_b = \zeta\chi_f$). The actuation force in terms of χ can be written as:

$$F_f^{em}(x, V) = \frac{\epsilon V^2}{z'} \lambda_{1,p} \lambda_{2,p} \frac{l_d^3}{x_p \sqrt{(4l_d^2 - {x_p}^2)}} f_f^{em}(\chi) \tag{20}$$

$$f_f^{em}(\chi) = \chi(\chi^2 - 2)$$

  that shows how the actuation force becomes null when the lozenge shaped EDF degenerates into a square EDF (i.e. for $\chi = \widetilde{\chi}_f = \sqrt{2}$ or $\widetilde{x}_f = \sqrt{2} l_d$) and eventually changes sign for $\chi \geq \sqrt{2}$. The function $f_f^{em}(\chi)$ is plotted in Fig. 15 and has a minimum for $\chi = \sqrt{2/3}$.
  Let us consider configurations of the EDF such that $\chi < \widetilde{\chi}_f$. Considering the EDF parameters as fixed and given a maximum actuation voltage V_{max}, then:

$$e_T^{diamond} = \frac{max_{\chi_b, \chi_f}(f_{em}(\chi))}{min_{\chi_b, \chi_f}(f_{em}(\chi))} \tag{21}$$

[2] In the following $max[f(x)]$within $x_b \leq x \leq x_f$ will be indicated as $max_{x_b, x_f}[f(x)]$

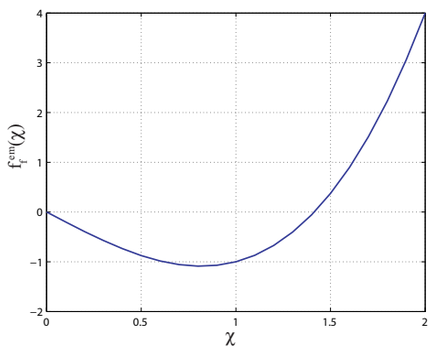

Fig. 15. Plot of $f_f^{em}(\chi)$

which is minimum if $f_{em}(\chi_b) = f_{em}(\chi_f)$, that is:

$$\chi_f = \sqrt{\frac{2}{\zeta^2 + \zeta + 1}} \tag{22}$$

The resulting force difference relative error being

$$e_T = \frac{\sqrt{8/3} - (2/3)^{\frac{3}{2}}}{2\chi_f - \chi_f^3} - 1 \tag{23}$$

Therefore, in order to minimize the force difference relative error, given x_b and x_f, l_d should be chosen such that:

$$l_d = \frac{x_f}{\sqrt{2}}\sqrt{\zeta^2 + \zeta + 1} \tag{24}$$

6. DE design constraints

In this section, three different types of design constraints or failure modes that can affect EDF design are described. These failure modes do not take into account the effect of localized material flaws, electric field concentrations or stress concentrations.

- *Mechanical failure*. This condition occurs when the mechanical strength of the material is exceeded. Experimental activities have shown that mechanical failure for hyperelastic polymers is primarily a function of stretch and not of stress and it takes place when folded polymer chains are straightened beyond their unfolded length. Plante (2006) reports a mechanical failure criterion based on DE film area expansion stating that failure is prevented if $A_{final}/A_{initial} < c$. The term $A_{initial}$ is the initial DE area before prestretch, A_{final} is the DE area at breaking and c is a characteristic constant. However, it has been shown (Vertechy et al., 2009) that also the Kawabata's failure criterion is suited for the study of DE materials and simpler to use when designing. This criterion (Hamdi et al., 2006) postulates that the mechanical failure of polymers under any loading path occurs when any principal stretch equals or exceeds the value of the stretch at break measured under uniaxial tension, that is:

$$max[\lambda_1, \lambda_2] \geq \lambda_{ut} \tag{25}$$

where λ_{ut} is the principal stretch at break achieved in an uniaxial test.

- *Electric breakdown*. This type of failure occurs when the electric field in a material becomes greater than its dielectric strength. In this situation the electric field may mobilize charges within the DE, producing a path of electric conduction. After electric breakdown, the DE will present a permanent defect preventing its usage for actuation. Electric breakdown occurs when:

$$E \geq E_{br} \tag{26}$$

  where E_{br} is the electric field at break that is usually determined experimentally. A theoretical prediction of electric breakdown can be found in Whithead (1953). For actuation usage, it is useful to activate the DE electric fields which are as close as possible to the electric field at break (indeed an higher E signifies higher F_f^{em}). Recent experiments have shown that DE prestretching increases the DE dielectric strength. For this reason, in the following design procedure DE prestretch is maximized.
- *Loss of tension*. This condition occurs when the applied voltage induces deformations which may remove the tensile prestress. In fact, EDF have negligible flexural rigidity. This thin membrane can wrinkle out of its plane under slight compressive stresses which arise if the applied voltage is too high and exceed the given prestretch. Loss of tension is avoided if:

$$\sigma_1 > 0 \; \forall \; \Omega(t); \qquad \sigma_2 > 0 \; \forall \; \Omega(t) \tag{27}$$

  where $\Omega(t)$ are the possible configurations of the DE film in working condition.
  Another cause of DE failure is electromechanical instability or *pull-in* (Stark & Garton, 1955) and was identified as a mean of dielectric failure in insulators in 1950 (Mason, 1959). Pull-in is not properly a failure mode but a phenomenon that can eventually lead to either mechanical failure or electric breakdown. In fact, a voltage application causes DE expansion and subsequent reduction of thickness. A reduction in thickness signifies higher electric fields. Therefore there exists a positive feedback between a thinner elastomer and a higher electric field. An unrestricted area expansion of the material may lead to mechanical failure whereas higher electric fields may lead to electric breakdown. As reported by Lochmatter (2007), however, this hypothesis has not yet been proven experimentally and the condition of Eqs. 25, 26, 27 are considered sufficient for design purposes.

7. Analytical model development for the Slider Crank Compliant Mechanism

The FL curve concerning a compliant mechanism can be found by the PRBM using either the principle of virtual work or the free-body diagram approach Howell (2001).
Supposing the pin joints being torsional linear springs, the torques due to the deflection of the springs are given by:

$$T_i = -K_i \Psi_i \tag{28}$$

where, with reference to Fig. 8(c), K_i, $i = 1,2,3$ are the pivot torsional stiffnessess to be designed and $\Psi_1 = \vartheta_1 - \vartheta_{10}$, $\Psi_2 = \vartheta_3 - \vartheta_{30} - \vartheta_1 + \vartheta_{10}$, $\Psi_3 = \vartheta_3 - \vartheta_{30}$. The following relationships are found from the position analysis of the mechanism:

$$\vartheta_3 = \pi - asin\Big(\frac{r_1 sin(\vartheta_1) - e}{r_2}\Big); \qquad x = r_1 cos(\vartheta_1) - r_2 cos(\vartheta_3); \qquad \alpha = atan(\frac{e}{x}) \tag{29}$$

If the value of the eccentricity e is such that $e = 0$, the law of cosines can be used leading to the following expressions:

$$\vartheta_1 = acos\left(\frac{x^2 + {r_1}^2 - {r_2}^2}{2xr_1}\right); \qquad \vartheta_3 = acos\left(\frac{x^2 + {r_2}^2 + {r_1}^2}{2xr_2}\right)$$

Note that, if the compliant mechanism is formed form a monolithic piece, then:

$$\vartheta_{30} = \pi - asin\left(\frac{r_1 sin(\vartheta_{10}) - e}{r_2}\right) \tag{30}$$

From the static analysis of the mechanism, the following FL relationship can be obtained:

$$F_s = F_1 + F_2 + F_3 \tag{31}$$

where

$$F_1 = \frac{K_1 \Psi_1 cos(\vartheta_3)}{r_1 sin(\vartheta_3 - \vartheta_1)}; \qquad F_2 = \frac{K_2 \Psi_2 cos(\alpha)}{r_1 sin(\vartheta_1 - \alpha)}; \qquad F_3 = \frac{K_3 \Psi_3 cos(\vartheta_1)}{x\ sin(\vartheta_1) - e\ cos(\vartheta_1)} \tag{32}$$

The same expressions holds when $e = 0$.
Let us define the variable $K_{12} = K_1/K_2$ and the function $\Xi = \Xi(K_{12}, r_1, r_2, e, \theta_{10})$ such that:

$$F_{12} = K_1 \Xi \tag{33}$$

where

$$\Xi = \frac{\Psi_1 cos(\vartheta_3)}{r_1 sin(\vartheta_3 - \vartheta_1)} + \frac{K_{12} \Psi_2 cos(\alpha)}{r_1 sin(\vartheta_1 - \alpha)} \tag{34}$$

This expression will find a use when designing the SCCM such that F_{12} is quasi constant along a given range of motion (see section 9.2)

8. Design procedure and actuator optimization

Let us derive a general design methodology, that can be used to optimize DELA whose analytical model is available. Nevertheless, in case the geometry of the DELA does not make it possible to derive simple mathematical models, the considerations which are drawn concerning the frame stiffness remain valid.

8.1 Design variables

The actuator available thrust, F_a, is given by Eq. 1. The maximum thrust in the OFF state mode is $F_{max}^{off} = F_a(x, 0)$. The maximum thrust in the ON state mode is $F_{max}^{on} = F_a(x, V_{max})$. The overall design of a DELA depends on numerous parameters. In practical applications some of these parameters are defined by the application requirements whereas some others are left free to the designer.
First of all, when a DE material is chosen for applications (silicone or acrylic DE (Kofod & Sommer-Larsen, 2005; Plante, 2006)), the material electromechanical properties are given, that is the dielectric constant ϵ_r, the constants related to the material constitutive equation, the electric field at breaking E_{br} and the ultimate stretch at breaking λ_{br}. Supposing to use an Ogden model for the DE constitutive equation and electrodes, the constants μ_p, α_p are given.
It is supposed that the actuator size is given along with the maximum encumbrance of the

actuator is determined by the application requirements. Moreover, the maximum actuation voltage V_{max} which can be supplied by the circuitry is given along with the DELA initial and final positions x_b, x_f ($\delta = x_b - x_f$ being the desired actuator stroke).

The designer can specify the maximum thrust profile in the OFF state mode $\overline{F}^{off}_{max}$ or the maximum thrust profile in the ON state mode $\overline{F}^{on}_{max}$, the thrust profile being approximated with a linear function with slope (stiffness) K_d. However it is wiser to specify the desired thrust profile in the OFF state mode because it depends on the DELA elastic properties only. The thrust in the ON state mode depends both on the elastic properties and on the applied voltage meaning that it can be controlled at will to a certain extent (using controllable actuation sources and sensory units). At last, the force difference $\Delta\overline{F}_a$ between $\overline{F}^{off}_{max}$ and $\overline{F}^{on}_{max}$ must be defined. Note that, as long as the frame is a passive elastic element, $\Delta F_a(x) = {F_f}^{off}(x) - {F_f}^{on}(x) = F^{em}_f(x)$.
Variables which are unknown at this stage are:

- The initial DE film dimensions x', y', z'. Due to the production techniques of the DE films (which are either purchased as thin films or obtained by injection moulding), it is likely that the film thickness z' cannot be chosen at will. However a stack of insulating DE films can be used to form a single DE. Therefore it will be assumed that $z' \in \mathbb{I}$, $\mathbb{I}$ being a given set of integer number, whereas x', y' are completely left free to the designer.
- The DE prestretches in the planar directions $\lambda_{1p}, \lambda_{2p}$. It should be underlined again that prestretch in some direction is necessary for the DE film not to wrinkle under actuation. In addition, prestretch increases the breakdown strength of DE films, therefore improving actuator performance (Kofod et al., 2003; Pelrine et al., 2000; Plante & Dubowsky, 2006). At last, the effect of prestretch is to alter the DE film dimensions making it thinner and wider and therefore increasing ΔF_f for a given voltage, V (for instance see Eqs. 8 and 16). Therefore prestretch should be kept as high as possible.
- The number of film layers N_{layers}.
- Concerning the SCCM used to correct the DELA stiffness every kinematic and structural variable is still unknown.

In summary:

- *Given data*:
  - **Material properties**.
    - DE mechanical properties: μ, α
    - DE stretch at break: λ_{br}
    - DE electrical properties: ϵ_r
    - Electric field at break: E_{br}
  - **Application requirements**.
    - Actuator planar dimensions (maximum allowable by application constraints);
    - Actuator initial and final position (and desired stroke): x_b,x_f;
    - Desired thrust profile: $\overline{F}^{off}_{max}$ (with approximately constant stiffness K_d);
    - Desired actuation force: $\Delta\overline{F}_a = \Delta\overline{F}_f$.
  - **Circuitry parameters**.
    - Maximum actuation voltage: V_{max};
- *Design variables*:
  - **DE film parameters**
    - DE film initial dimensions: x', y', z' where $z' \in \mathbb{I}$;

- Amount of prestretch: $\lambda_{1p}, \lambda_{2p}$;
- Number of film layers: N_{layers}.

• **Frame parameters.**

- Links lengths and dimensions: r_1, r_2, e;
- Flexural pivot dimensions: $K_i,\ i = 1, 3$ and θ_{10}.

8.2 The design procedure

The design procedure comprises two steps: first the determination of the DE geometrical parameters, second the design of the flexible frame.

• **Determination of the DE geometrical parameters**

1. Choose a suitable DE geometry and define the actuator planar dimensions which are compatible with the application constraints.
   Recall that, for the diamond actuators, given the desired initial and final actuator lengths, x_b and x_f, it is possible to choose the lozenge length that minimizes the force difference error e_T. Minimizing this error means that F_f^{off} and F_f^{on} are close to parallel in the $x_b - x_f$ range. The same result cannot be achieved with rectangular actuators, where e_T is independent of the actuator geometrical parameter y_p.
2. Given x_b, x_f (and therefore y_b, y_f), the ultimate stretch at break λ_{br} and a suitable safety factor ϕ_λ to avoid mechanical break, find the initial DE film planar dimensions, x', y':

$$\lambda_{1max} = \frac{x_f}{x'} = \phi_\lambda \lambda_{br} \Rightarrow x' = \frac{x_f}{\phi_\lambda \lambda_{br}} \qquad \lambda_{2max} = \frac{y_b}{y'} = \phi_\lambda \lambda_{br} \Rightarrow y' = \frac{y_b}{\phi_\lambda \lambda_{br}} \tag{35}$$

3. Given x', y', find $\lambda_{1p}, \lambda_{2p}$:

$$\lambda_{1,p} = \frac{x_b}{x'}; \qquad \lambda_{2,p} = \frac{y_b}{y'} \tag{36}$$

4. Given $x', y', x_f, y_f,\ V_{max}$, the electric field at break E_{br} and a suitable safety factor to avoid electrical break ϕ_{el}, find z':

$$E_{max} = \phi_{el} E_{br} = \frac{V_{max}}{z_{min}} \Rightarrow z_{min} = \frac{V_{max}}{\phi_{el} E_{br}} = z_f \tag{37}$$
$$\lambda_{3min} = \frac{z_f}{z'} \Rightarrow z' = \frac{z_f}{\lambda_{3min}} = \frac{V_{max}}{\phi_{el} E_{br}} max_{x_b, x_f}(\lambda_1 \lambda_2)$$

   Choose $\widetilde{z}' \in \mathbb{I}$ such that $\widetilde{z}' \geq z'$
5. Given the aforementioned quantities, the quantity $min\ F_f^{em}(x) = \Delta F_f^{min}$ within $x_b \leq x \leq x_f$ can be analytically computed for one layer of film. Knowing the desired $\Delta \overline{F}_f$, find N_{layer} such that:

$$N_{layer} \Delta F_f^{min} \geq \Delta \overline{F}_f \tag{38}$$

6. Verify that $\sigma_i > 0\ \forall\ \Omega(t),\ i = 1, ...2$. If the condition is not verified, decrease V_{max} and, in case, increase N_{layer} in order to achieve the desired thrust.

• **Design of the flexible frame**

1. Impose the UEP at a point $\overline{x}$ such that $x_b \leq \overline{x} \leq x_f$. The imposition of the UEP at a given $\overline{x}$ constrains the dimension of either r_1 or r_2, for instance:

$$r_2 = \sqrt{r_1^2 + \overline{x}^2} \tag{39}$$

2. Considering Eq. 39, the frame force due to the torsional springs K_1, K_2 is given by

$$F_{1,2} = K_1 \Xi(K_{12}, r_1, e, \theta_{10}) \tag{40}$$

where $K_{12} = K_2/K_1$.
Use multivariable optimization (Howell, 2001) to find $K_{12}, r_1, e, \theta_{10}$ which minimize:

$$\Im = \frac{max_{x_b,x_f} \Xi}{min_{x_b,x_f} \Xi} \tag{41}$$

subjected to:

$$K_{12} \geq 0; \quad 0 < r_1^{min} < r_1 < r_1^{max}; \quad 0 \leq e^{min} < e < e^{max}; \quad \theta_{10}^{min} \leq \theta_{10} \leq \theta_{10}^{max} \tag{42}$$

The variable K_{12} and the connecting rod length r_1 are constrained to be positive. In addition the maximum and minimum values for r_1 and for the eccentricity e might be imposed by the application constraints. At last θ_{10} is allowed to vary in the range $[\theta_{10}^{min}, \theta_{10}^{max}]$ only, in order to avoid excessive deflections of the elastic joints.

3. Given the desired thrust profile $\overline{F}_{max}^{off}$ and therefore $\overline{F}_f^{off}(\overline{x})$, find K_1 such that

$$F_{1,2} - \overline{F}_f^{off}(\overline{x}) \approx 0 \tag{43}$$

4. Given K_{12} and K_1 then $K_2 = K_{12}K_1$

5. Given the DELA desired stiffness $K_d = \frac{dF_f^{off}(x)}{dx} \approx const$ find K_3 such that

$$K_3 + K_d \approx 0 \tag{44}$$

6. Given the values of K_i, $i = 1, 2, 3$ the designer can find the flexure dimensions. Supposing, for instance, the flexures are straight beam hinges with rectangular cross section then $K_i = \frac{EI_{a_i}}{L_i}$ where E is the frame material Young modulus, L_i is the length of the small-length flexural pivot, and $I_{a_i} = \frac{{h_i}^3 b_i}{12}$ is the moment of inertia of the pivot cross sectional area with respect to the axis a_i (h_i and b_i denotes the pivot thickness and width respectively, whereas a_i is the barycentric axis parallel to the width direction).

9. Case studies

9.1 Single-acting constant-force actuator of rectangular geometry

The objective of the present case study is to design a single-acting actuator capable of supplying a positive constant force over a given range of motion. The EDF is a Silicone DE (Whacker Elastosil RTV 625) coated with silver grease electrode (CW7100) (Kofod & Sommer-Larsen, 2005) and coupled to the rigid links containing the points O and P of the compliant frame schematized in Fig. 1(d). Displacement along the y direction (or, alternatively, rotation) of the rigid link containing the point O is prevented by the symmetry of both the compliant frame geometry and the EDF stress distribution.

- *Given data*:
  - **Material properties** (Kofod & Sommer-Larsen, 2005):
    $\mu = 596kPa$, $\alpha = 0.85$, $\lambda_{br} = 2$, $\phi_\lambda = 0.75$, $\epsilon_r = 2.7$, $E_{br} = 140MV/m$, $\phi_{el} = 0.7$
  - **Application requirements and Circuitry parameters**:
    $x_b = 16mm$, $x_f = 22mm$, $y_p = 43mm$ (Fig. 13(c)), $\overline{F}^{off}_{max} = 0.25N$, $\Delta\overline{F}_a = 0.25N$, $V_{max} = 2.5kV$
- *Design variables*:
  - impose $e = 0$, $\overline{x} = x_b$
  - **DE film parameters**:
    $x' = 14.6mm$, $y' = 28.6mm$, $z' = 0.5mm$, $\lambda_{1p} = 1.09$, $\lambda_{2p} = 1.5$, $N_{layers} = 2$;
  - **Frame parameters.**:
    $r_1 = 21.5mm$, $r_2 = 26.8$, $e = 0mm$, $\theta_{10} = 22^\circ$
    $K_1 = 0.002Nm/rad$, $K_2 = 0.0034Nm/rad$, $K_3 = 0.067Nm/rad$

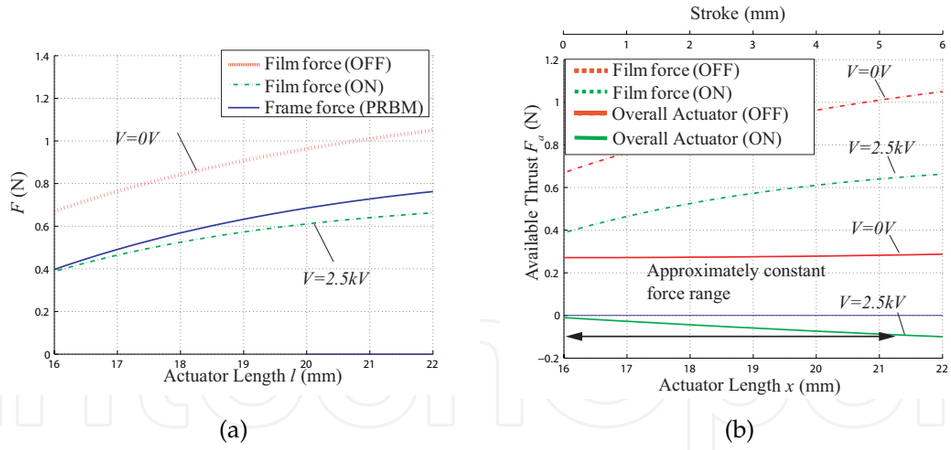

Fig. 16. Analytical FL relationship showing film force F_f and frame force absolute value $|F_s|$ (a), DE actuator FL curves when coupled with the delta element (final design) (b).

Figure 16(a) shows the frame force $|F_s|$ and the theoretical film forces F_f^{off}, F_f^{on} as functions of the actuator length x. The frame behavior is as expected. Figure 16(b) shows the film force F_f compared to the overall actuator available thrust F_a. The actuator thrust in the OFF state mode is approximately constant over the range 16-22 mm with value 0.27 (in this range a maximal deviation by 0.01 N is admitted).

9.2 Bidirectional constant-force actuator of diamond shape

Objective of the present case study is the design of a bidirectional constant-force actuator of diamond shape using a compound-structure flexible frame. The EDF is an acrylic DE (VHB 4905) coated with silver grease electrodes (CW7100) (Plante, 2006) and coupled with the four bar linkage mechanism schematized with a dashed line in Fig. 1(e).

- *Given data*:
  - **Material properties** (Kofod & Sommer-Larsen, 2005; Vogan, 2004):
    $\mu = 60kPA$, $\alpha = 1.8$, $\lambda_{br} = 8$, $\phi_\lambda = 0.63$, $\epsilon_r = 4.7$, $E_{br} = 150MV/m$, $\phi_{el} = 0.8$
  - **Application requirements and Circuitry parameters**:
    $x_b = 20mm$, $x_f = 30mm$, $l_d = \frac{x_f}{\sqrt{2}}\sqrt{\zeta^2+\zeta+1} = 30.8mm$ (Fig. 13(c)), $\overline{F}^{off}_{max} = 0.25N$, $\Delta\overline{F}_a = 0.5N$, $V_{max} = 7kV$
- *Design variables*:
  - impose $e = 0$, $\overline{x} = x_m = (x_f + x_b)/2$
  - **DE film parameters**:
    $x' = 6mm$, $y' = 31.74mm$, $z' = 1.5mm$, $\lambda_{1p} = 3.3$, $\lambda_{2p} = 5$, $N_{layers} = 1$
  - **Frame parameters.**:
    $r_1 = 21.5mm$, $r_2 = 33$, $e = 0mm$, $\theta_{10} = 10^\circ$
    $K_1 = 0.002Nm/rad$, $K_2 = 0.008Nm/rad$, $K_3 = 0.050Nm/rad$

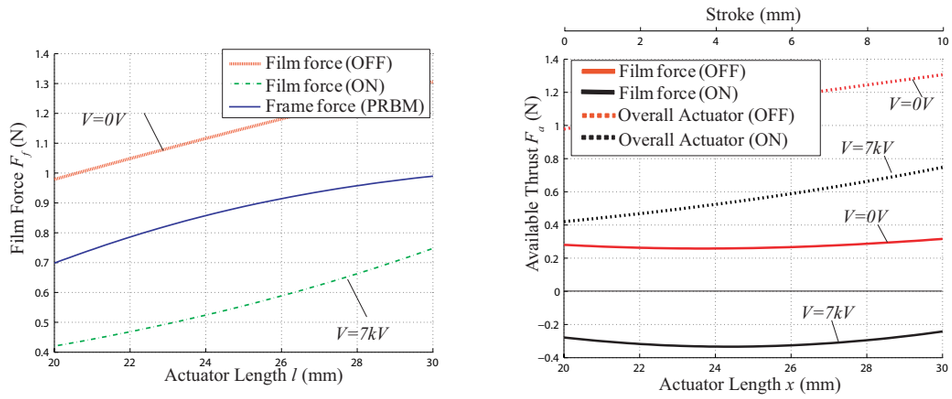

(a) (b)

Fig. 17. Analytical FL relationship showing film force F_f and frame force absolute value $|F_s|$ (a), DE actuator FL curves when coupled with the delta element (final design) (b).

Figure 17(a) shows the frame force $|F_s|$ and the theoretical film forces F_f^{off}, F_f^{on} as functions of the actuator length x. The frame behavior is as expected. Figure 17(b) shows the film force F_f compared to the overall actuator FL curve (compound-structure frame coupled with the DE film). The available thrust in the OFF state mode keeps a value close to 0.25N over the range 20-30 mm (in this range a maximal deviation by 0.008 N is admitted). In order to prevent the actuator from working in the non-linear range, mechanical stops can be provided.

9.3 DELA of Conical Shape with predetermined stiffness

The properties of the SCCM can also be used to modify the behavior of axialsymmetric actuators. As an example consider the conical actuator depicted in Fig. 18

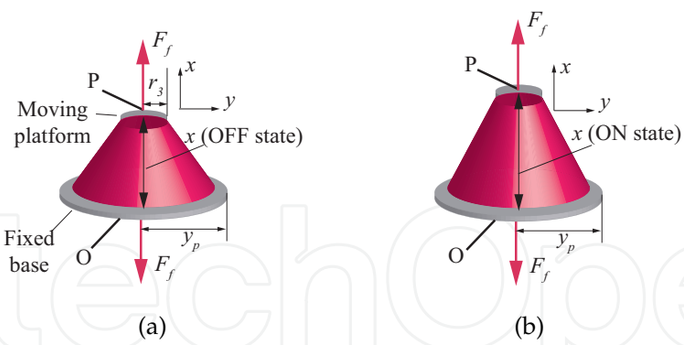

Fig. 18. Conical Actuator. OFF state mode (a), ON state mode (b).

Alike the other DELA geometries, the conical actuator supplies an available thrust that heavily changes along the stroke. This behavior is hereafter modified by coupling the conical EDF with the compliant frame shown in Fig. 1(f). The active film is shaped as a truncated cone. A planar circular DE film with initial radius of y' is first subjected to an equibiaxial prestretch up to a final radius denoted as y_p. Then, the application of an external force in the z direction (which is supplied by the moving platform of the compliant frame, see Fig. 1(f)) causes the DE film to gain a shape which is approximately conical. In this case, a simple mathematical model for the EDF is not available therefore the first part of the design procedure (concerning DE film design) cannot be employed. It should be stated, however, that a numerical solution of the conical DE has been proposed very recently by He et al. (2008). This solution relies on a set of differential equations to be solved numerically. Alternatively, FEM analysis can be used. In this work, the EDF FL curves have been determined experimentally using the procedure outlined in Berselli et al. (2009b). The EDF is an acrylic DE (VHB4905) coated with silver grease electrodes (CW7100). The objective of the present case study is to design a DELA capable of returning to an initial rest position when deactivated, that is to present a positive given stiffness K_d in the OFF state mode.

- *Given data*:
  - **DE film FL curve are determined experimentally; cone dimensions given below (Fig. 18)** (Berselli et al., 2009b)
    $y' = 20mm$, $y_p = 80mm$, $' = 1.5mm$, $r_3 = 12mm$
  - **Application requirements and Circuitry parameters**:
    $x_b = 20mm$, $x_f = 30mm$ (Fig. 13(c)), $\overline{F}^{off}(x) = 0.07x$, $\Delta\overline{F}_a = 1.5N$, $V_{max} = 5kV$
- *Design variables*:
  - impose $e = 28$, $\overline{x} = x_b$
  - **DE film parameters**:
    $x' = 6mm$, $y' = 31.74mm$, $z' = 1.5mm$, $\lambda_{1p} = 3.3$, $\lambda_{2p} = 5$, $N_{layers} = 1$
  - **Frame parameters.**:
    $r_1 = 20.9mm$, $r_2 = 21.2$, $e = 28mm$, $\theta_{10} = 42^\circ$
    $K_1 = 0.013Nm/rad$, $K_2 = 0.006Nm/rad$, $K_3 = 0.036Nm/rad$

In Figure 19(a), the modulus of the frame force $|F_s|$ and the film force F_f are plotted as functions of the actuator length x. The frame behavior is as expected. Figure 19(b) shows the the overall actuator available thrust F_a. The actuator thrust in the OFF state mode is a linear curve

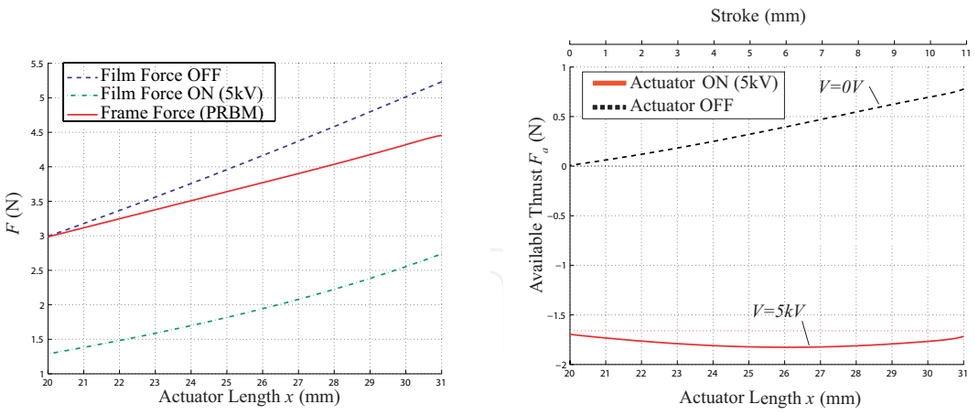

(a) (b)

Fig. 19. Analytical FL relationship showing film force F_f and frame force absolute value $|F_s|$ (a), DE actuator FL curves when coupled with the delta element (final design) (b).

vanishing at an actuator length of 20mm whereas the actuator thrust in the ON state mode is approximately constant (about 1.7N) over the range 20-30mm (in this range a maximal deviation by 0.1 N is admitted). A positive slope of the available thrust in the OFF state mode enables the actuator to come back to its initial rest position when deactivated.

10. Conclusions

The study of compliant actuators based on Dielectric Elastomers has been presented in a general framework which takes into account the interaction between the EDF and the film supporting frame. The key motivation of this work is based on the observation that a DELA presents an available thrust profile which can be heavily improved in terms of stiffness characteristics. Therefore, an easy methodology is needed to tailor the actuator stiffness to the application requirements.
In conclusion, the main contributions of this chapter can be summarized as it follows:

- A novel concept for the design of compliant frames has been proposed. The concept makes use of the stiffness properties of the slider-crank compliant mechanism. If suitably coupled with EDF of different geometries, such mechanism permits to adjust the DELA available thrust profile at the will of the designer.
- A novel design methodology has been presented which allows to tailor the stiffness of the actuator to the application requirements, defining its structural and geometrical properties. The procedure is composed of two main sub-procedures, one allowing the design of the EDF, the other one allowing the design of the compliant frame. In particular, the first part of the procedure can be employed to size EDF which are shaped as lozenges or rectangles for which analytical models are available. It is not applicable to general DE geometries (which require resorting to FEM analysis or experiments). The second part of the procedure is general and can be used to size the compliant frames even if a mathematical model of the EDF is not directly available.
- Three case studies have been presented concerning rectangular shaped EDF, lozenge shaped EDF, and conically shaped EDF. The response of the rectangular-shaped and

lozenge-shaped EDF have been determined analytically. The response of the conical-shaped EDF have been determined experimentally. Every geometry is coupled with a suitable compliant frame.

11. Acknowledgment

This research has been partially funded by Mectron Laboratory, Regione Emilia Romagna.

12. References

Bar-Cohen, Y. (2004). *Electroactive Polymer (EAP) Actuators as Artificial Muscles: Reality, Potential and Challenges*, Vol. PM136 of 2, SPIE Press.

Berselli, G., Vertechy, R., Vassura, G. & Parenti Castelli, V. (2008). A compound-structure frame for improving the performance of a dielectric elastomer actuator, *Springer, Advances in Robot Kinematics* **11**: 391–398.

Berselli, G., Vertechy, R., Vassura, G. & Parenti Castelli, V. (2009a). Design of a single-acting constant-force actuator based on dielectric elastomers, *ASME Journal of Mechanisms and Robotics, to be published* .

Berselli, G., Vertechy, R., Vassura, G. & Parenti Castelli, V. (2009b). Experimental evaluation of optimal conically-shaped dielectric elastomer linear actuators, *Intelligent Robots and Systems, 2009. IROS 2008. IEEE/RSJ International Conference on* .

Biagiotti, L., Tiezzi, P., Melchiorri, C. & Vassura, G. (2004). Modelling and controlling the compliance of a robotic hand with soft finger-pads, *IEEE Int. Conf. on Robotics and Automation, ICRA, Workshop on Multi-point Interaction in Robotics and Visrtual Reality*, New Orleans, LA.

Bicchi, A. & Tonietti, G. (2004). Fast and soft arm tactics: Dealing with the safety-performance tradeoff in robot arms design and control., *IEEE Rob. Aut. Mag.* **11**: 22–33.

Biddiss, E. & Chaua, T. (2008). Dielectric elastomers as actuators for upper limb prosthetics: Challenges and opportunities, *Medical Engineering and Physics* **30**(4): 403–418.

Bolzmacher, C., Hafez, M., Khoudja, M. B., Bernardoni, P. & Dubowsky, S. (2004). Polymer based actuators for virtual reality devices and rehabilitation applications, *Proceedings of the SPIE*, Vol. 5385, pp. 281–289.

Hamdi, A., Nait Abdelaziz, M., Ait Hocine, N., Heuillet, P. & Benseddiq, N. (2006). A fracture criterion of rubber-like materials under plane stress conditions, *Polymer Testing* **25(8)**: 994–1005.

He, T., Zhao, X. & Suo, Z. (2008). Equilibrium and stability of dielectric elastomer membranes undergoing inhomogeneous deformation, *Available online* .

Howell, L. (2001). *Compliant Mechanisms*, John Wiley and Sons.

Jung, K., Kima, K. J. & Choi, H. R. (2008). A self-sensing dielectric elastomer actuator., *Sensors and Actuators A* **143**: 343–351.

Kim, L. K. & Tadokoro, S. (2007). *Electroactive Polymers for Robotic Applications: Artificial Muscles and Sensors*, Eds. Springer.

Kofod, G., Paajanen, M. & Bauer, S. (2006). Self-organized minimum-energy structures for dielectric elastomer actuators, *Applied Physics A: Materials Science and Processing* **85(2)**: 141–143.

Kofod, G. & Sommer-Larsen, P. (2005). Silicone dielectric elastomer actuators: Finite-elasticity model of actuation, *Sensor and Actuators* **122**: 273–283.

Kofod, G., Sommer-Larsen, P., Kornbluh, R. & Pelrine, R. (2003). Actuation response of polyacrylate dielectric elastomers, *Journal of Intelligent Material Systems and Structures* **14**: 787–793.

Kornbluh, R. ., Pelrine, R. & Joseph, J. (1995). Dielectric artificial muscle actuators for small robots, *Proceedings of the Third IASTED International Conference on Robotics and Manufacturing, Cancun, Mexicoe*.

Koseki, Y., Tanikawa, T. & Chinzei, K. (2007). MRI-compatible micromanipulator-design and implementation and MRI-compatibility tests, *Proc. of EMBC 2007*, pp. 465–468.

Lochmatter, P. (2007). *Development of a Shell-like Electroactive Polymer (EAP) Actuator*, PhD thesis, Federal Institute of Technology, Zurich.

Mason, J. (1959). *Dielectric Breakdown in Solid Insulation*, Progress in Dielectrics I, Heywood and Company Ltd.

Ogden, R. W. (1972). Large deformation isotropic elasticity: on the correlation of theory and experiment for incompressible rubber-like solids, *Proc. Roy. Soc. London* **A-326**: 565–584.

Paul, R. & Shimano, B. (1976). Compliance control., *Proceedings of the JACC*.

Pedersen, C. B. W., Fleck, N. A. & Ananthasuresh, G. K. (2006). Design of a compliant mechanism to modify an actuator characteristic to deliver a constant output force, *Journal of Mechanical Design* **128**(5): 1101–1112.

Pei, Q., Pelrine, R., Standford, S., Kornbluh, R. & Rosenthal, M. (2003). Electroelastomer rolls and their application for biomimetic walking robots, *Synth. Met.* **135/136**: 129–131.

Pelrine, R., Kornbluh, R. & Joseph, J. (1998). Electrostriction of polymer dielectrics with compliant electrodes as a means of actuation, *Sensors Actuators A* **64**: 77–85.

Pelrine, R., Kornbluh, R. & Kofod, G. (2000). High-strain actuator materials based on dielectric elastomers, *Advanced Materials* **12(16)**: 1223–1225.

Plante, J. S. (2006). *Dielectric elastomer actuators for binary robotics and mechatronics*, PhD thesis, Department of Mechanical Engineering, Massachusetts Institute of Technology, Cambridge, MA.

Plante, J. S. & Dubowsky, S. (2006). Large-scale failure modes of dielectric elastomer actuators, *Int. J. Solids Struct.* **43**.

Plante, J. S. & Dubowsky, S. (2008). MRI compatible needle manipulator for robotic assisted interventions to prostate cancer, *in* F. Carpi & E. Smela (eds), *Biomedical applications of electroactive polymer actuators*, Wiley.

Stark, K. H. & Garton, C. G. (1955). Electric strength of irradiated polythene, *Nature* **176**: 1225–1226.

Toupin, R. A. (1956). The elastic dielectrics, *J. Rational Mech. Anal.* **5**: 849–915.

Vertechy, R., Berselli, G., Vassura, G. & Parenti Castelli, V. (2009). A new procedure for the optimization of a dielectric elastomer actuator, *Springer, Computational Kinematics* **1**: 391–398.

Vogan, J. (2004). *Development of dielectric elastomer actuators for MRI devices*, Master's thesis, Department of Mechanical Engineering, Massachusetts Institute of Technology, Cambridge, MA.

Whithead, S. (1953). *Dielectric Breakdown of Solids*, Oxford University Pres.

Williamson, M. M. (1993). *Series elastic actuators*, Master's thesis, Department of Electrical Engineering and Computer Science, Massachusetts Institute of Technology, Cambridge, MA.

Wingert, A., Lichter, M. D. & Dubowsky, S. (2006). On the design of large degree-of-freedom digital mechatronic devices based on bistable dielectric elastomer actuators, *IEEE/ASME Transactions on Mechatronics* **11**(4): 448–456.

Robot Manipulators New Achievements

Edited by Aleksandar Lazinica and Hiroyuki Kawai

ISBN 978-953-307-090-2
Hard cover, 718 pages
Publisher InTech
Published online 01, April, 2010
Published in print edition April, 2010

Robot manipulators are developing more in the direction of industrial robots than of human workers. Recently, the applications of robot manipulators are spreading their focus, for example Da Vinci as a medical robot, ASIMO as a humanoid robot and so on. There are many research topics within the field of robot manipulators, e.g. motion planning, cooperation with a human, and fusion with external sensors like vision, haptic and force, etc. Moreover, these include both technical problems in the industry and theoretical problems in the academic fields. This book is a collection of papers presenting the latest research issues from around the world.

InTech Europe
University Campus STeP Ri
Slavka Krautzeka 83/A
51000 Rijeka, Croatia
Phone: +385 (51) 770 447
Fax: +385 (51) 686 166
www.intechopen.com

InTech China
Unit 405, Office Block, Hotel Equatorial Shanghai
No.65, Yan An Road (West), Shanghai, 200040, China
中国上海市延安西路65号上海国际贵都大饭店办公楼405单元
Phone: +86-21-62489820
Fax: +86-21-62489821

IntechOpen